Available online at www.sciencedirect.com
SCIENCE DIRECT
Cement and Concrete Research 35 (2005) 1495–1502
Cement and Concrete Research

Statistical modeling of the geometrical structure of the system of artificial air pores in autoclaved aerated concrete

Ilja Kadashevich[a], Hans-Jürgen Schneider[b], Dietrich Stoyan[a,*]

[a]Institute of Stochastics, Freiberg University of Mining and Technology, 09596 Freiberg, Germany
[b]Institute of Ceramics, Glass and Construction Materials, Freiberg University of Mining and Technology, 09596, Germany

Received 25 March 2004; accepted 12 October 2004

Abstract

The geometrical structure of the system of artificial air pores in autoclaved concrete is studied, based on samples from laboratory and industry. The single pores are approximated by spheres, the corresponding radius distribution is determined by means of stereological methods. The resulting distribution is not a classical standard distribution, but instead requires a mixture of three components, one of them Gaussian. The pore system as a whole is approximated by the penetrable-concentric-shell or "cherry-pit" model, which consists of spheres that are partially penetrable. The corresponding hard cores form a random packing of hard spheres. The goodness-of-fit of the model is tested by means of information available from planar sections: the section profile radius distribution and the pair correlation function of profile centers.

Keywords: Image analysis; Pore size distribution; Modeling; Particle packing

1. Introduction

Autoclaved aerated concrete (AAC) is an important construction material of a rather complicated microstructure. Between 60% and 90% of its volume consists of pores, which are classified as micro and macro capillaries and artificial air voids and have diameters between some 100 nm and 4 mm [1–4]. As for many materials, the microstructure of AAC has great influence on bulk properties such as strength, toughness, moisture transport, and heat transfer [5,6]. In the case of AAC, it is well known that the most important material parameter is porosity or bulk density and that the 'degree of inhomogeneity' of the geometrical pore structure plays a significant role [7]. It is clear that for theoretical studies of bulk properties of AAC, a precise geometrical model of its microstructure is needed. Though there are many papers about voids and their structure in AAC [1,3,4,8,9], the authors are aware of only one paper on a stochastic model which can be used for computer simulation: the unpublished PhD thesis of He [10], in which a random dense packing of spheres was suggested as a model for the system of artificial air pores.

The aim of the present paper is to describe a geometrical model for the system of artificial air pores (larger than 25 μm and smaller than 1 mm in radius). It starts from the usual assumption that single pores are spherical. The pore radii are variable and the corresponding radius distribution plays an important role. Based on the analysis of a series of AAC samples including image analysis of planar sections [11], a parameterized family of radius distributions is introduced. For the spatial arrangement of the pores, the well-known penetrable-concentric-shell or "cherry-pit" model [5,12,23] is used, i.e., it is assumed that the spheres, which stand for the pores, are randomly distributed in space and are partly (but not fully) penetrable. This model can be easily simulated and is therefore useful for future investigations of bulk properties of AAC. Comparison with samples of AAC shows that the model yields a good fit.

* Corresponding author. Tel.: +49 3731 39 2118; fax: +49 3731 39 3598.
E-mail address: stoyan@orion.hrz.tu-freiberg.de (D. Stoyan).

0008-8846/$ - see front matter © 2004 Elsevier Ltd. All rights reserved.
doi:10.1016/j.cemconres.2004.10.010

2. Materials

Modern AACs have porosities between 60% and 90%, which correspond to bulk densities between 1 and 0.3 g/cm^3 [4,8]. Their pores form complicated geometrical structures with pore sizes usually smaller than 1 mm in radius. It is possible to control the porous structure by the raw material.

Two series of AAC samples were investigated, one produced in the laboratory of the Institute of Ceramics, Glass and Construction Materials of Freiberg University of Mining and Technology and the other in the Schrobenhausen of Xella Baustoffe, Germany, plant.

The samples produced in Freiberg differ with respect to porosity, which ranges between 69% and 86%; but there are also samples of the same porosity but with different mean pore sizes. All these samples were produced under identical physical conditions; the structural differences result from quantity or type of powdered aluminium as pore agent. The raw material composition was arenaceous quartz (SiO_2) 68.5%, lime and portland cement (CaO) 30.0% and anhydrite ($CaSO_4$) 1.5%. The water to solid relationship was 0.6 kg/kg. All components were mixed in water for 5 min and then the expansion process was initiated. After 2 h, the prismatic, still plastic bodies were demoulded and hardened for 12 h in an autoclave at 191 °C and 1.3 MPa overpressure [13]. The final AAC bodies were prisms of size 200×200×250 mm.

The industry samples of commercial aerated concrete were blocks of 199×240×499 mm. Their porosities lay between 71.4% and 86.4%, and the apparent solid densities were between 0.35 and 0.75 g/cm^3.

This paper reports on four typical AAC specimens, three from the laboratory and one from industry, which are considered as representative for the whole set of samples. They are denoted in the following as A, B, C, and D (the industry probe PP2-0,35 according to DIN 4165, with a porosity of 86.34%). The sample properties are presented in Table 1.

3. Experimental

3.1. Cutting of AAC samples

From all AAC samples, three cubic samples for each type of concrete were taken. Since the structure of AAC changes in the expansion direction [14,15], the samples were cut out from the interior of the AAC bodies. Sample orientation followed the direction of expansion, which is taken as the vertical direction. The cubes were cut out with a precision machine with diamond a cut-of wheel, the specimens were wet-ground so the sides were flat and parallel and the final cube side was 55 mm. The dimension of tolerance was <0.1 mm on 100 mm. Finally, the cubes were dried at 50 °C until mass constancy. Fig. 1 shows two typical cubes.

Table 1
Parameters of the AAC porous structure for four samples

Samples	Pure density ρ, g/cm^3	Bulk density ρ_R, g/cm^3	P, %	P_{Air}, %	$P_{Capillary}$, %	P_{Cracks}, %
A	2.632	0.814	69.07	16.56	47.43	5.08
B	2.632	0.485	81.57	52.99	26.72	1.86
C	2.632	0.535	79.67	43.97	31.85	3.85
D	2.592	0.350	86.34	64.46	20.20	1.68

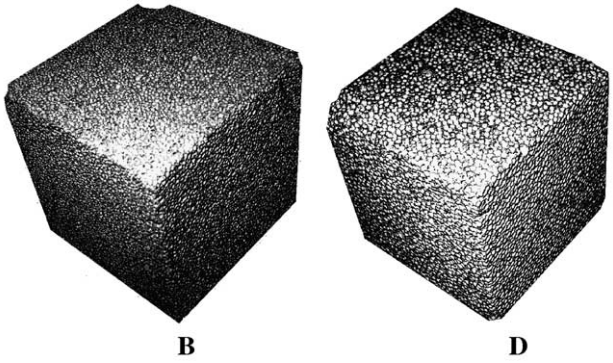

Fig. 1. AAC sample cubes of types B and D.

3.2. Measuring material characteristics

For all AAC samples, bulk density ρ_R, skeletal density (or true density) ρ, and porosity P were determined. Bulk density was measured according to DIN EN 678 by geometrical measurement, drying at 105 °C until mass constancy and final weighing. Skeletal density was determined by means of a helium pycnometer; before, the AAC samples were comminuted to particles smaller than 63 μm. Porosity is then obtained, under assumption that the mass of air in the sample is zero, as:

$$P = \left(1 - \frac{\rho_R}{\rho}\right) 100\%. \quad (1)$$

Table 1 shows these values for the four samples which are discussed in this paper.

3.3. Preparation of samples for image analysis

An important condition for successful application of image analysis in the statistical analysis of the geometrical structure of the surfaces of specimen is a sufficient black and white contrast between pores (white) and matrix (black). After cutting the AAC material into cubes, the sampling surfaces, which were taken perpendicular to the expansion direction, were prepared for the investigation. The steps are: dry fine-grinding by means of abrasive paper of granulation class 800 (following DIN 69 100), removal of debris, careful black coloring with water-resistant alcohol-based ink and filling of the pores with hydrated aluminum powder. The fineness of the powder (0.1–2.5 μm) and of the

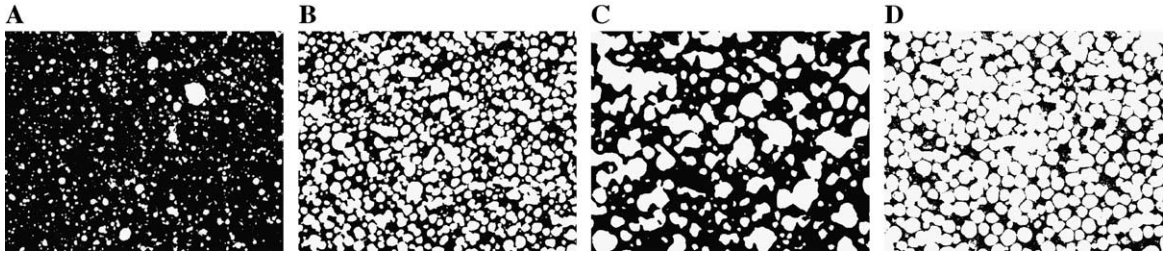

Fig. 2. Binary images of the four AAC samples (30×24 mm).

abrasive paper ensures correct images of the circular pores up to 50 μm diameter. The images were then taken with the macro objective, following the reflected light method.

3.4. Basic steps of image analysis

The prepared surfaces of sample cubes were processed using an Image-C MATAM software of IMTRONIC and converted into bitmaps. Fig. 2 shows binary images for the four analyzed cubes.

The first step of image analysis is determination of porosity on the surfaces, i.e., of the area fraction P_{Air} of the white phase of samples as in Fig. 2. Here P_{Air} is that part of porosity which results from (nearly) spherical air voids. Rare defects such as cracks and huge air bubbles (larger than 1 mm in radius) are summarized in P_{Cracks}. This part cannot be modeled by the model described in Section 4 and will be ignored. (However, in principle, huge air bubbles can be easily added to the spheres of the proposed packing model.) The value P_{Air} is very important for model fitting, because it will serve as a target parameter. The difference $P_{\mathrm{Capillary}}=P-P_{\mathrm{Air}}-P_{\mathrm{Cracks}}$ corresponds to pores smaller than 50 μm, which are often called micro and macro capillaries.

In the second step, the porous (white) phase is approximated by a system of overlapping disks. A special software was used for this task, which is based on the open source image analysis library IPL98 [16]. The main idea of the algorithm is sketched in Fig. 3. In the first step, isolated agglomerates of voids are determined (a) and then divided into single voids (b). For the resulting voids, "centers" are determined as centers of gravity and then disks with these centers are constructed so that the area of the set-theoretic union of disks is equal to the area of voids (c). The resulting radii are denoted as r_i. Fig. 4 shows the resulting approximating disk systems for the four samples.

In the third step, the pair correlation functions (PCFs) g_{A} [17] for the planar point patterns of disk centers are determined. They describe in some way the spatial variability of the arrangement of voids and serve later for model parameter choice. Fig. 9 in Section 6 below will show such functions.

4. Methods

4.1. Stereological determination of sphere radius distribution

In the proposed three-dimensional model of AAC, the voids are approximated as spheres. The corresponding radius distribution, which is given by the probability density function $\delta_{\mathrm{V}}(r)$, has to be chosen close to reality. It is determined here statistically, where the initial data are the disk radii of the constructed section profiles D_k as in Fig. 3.

Thus, one is confronted with the classical Wicksell problem [18–20]. This problem consists of the determination of the probability density function $\delta_{\mathrm{V}}(r)$ of the sphere radii, based on the probability density function $\delta_{\mathrm{A}}(r)$ of the radii of the corresponding circles of intersection, if the sphere system is intersected by a plane. Of course, the surfaces of sample cubes are considered as (parts of) planes through the AAC bodies. It is well known in stereology [18–20] that the relationship between $\delta_{\mathrm{A}}(r)$ and $\delta_{\mathrm{V}}(r)$ is given by the stereological equations:

$$\delta_{\mathrm{V}}(r) = -\frac{2rN_{\mathrm{A}}}{\pi N_{\mathrm{V}}}\int_r^\infty \frac{1}{\sqrt{x^2-r^2}}\frac{\mathrm{d}}{\mathrm{d}x}\left[\frac{\delta_{\mathrm{A}}(x)}{x}\right]\mathrm{d}x \tag{2}$$

and

$$\delta_{\mathrm{A}}(r) = r\frac{N_{\mathrm{V}}}{N_{\mathrm{A}}}\int_r^\infty \frac{\delta_{\mathrm{V}}(x)}{\sqrt{x^2-r^2}}\mathrm{d}x. \tag{3}$$

Here, N_{V} and N_{A} are the mean numbers of spheres and disks, respectively, per unit volume and area, respectively.

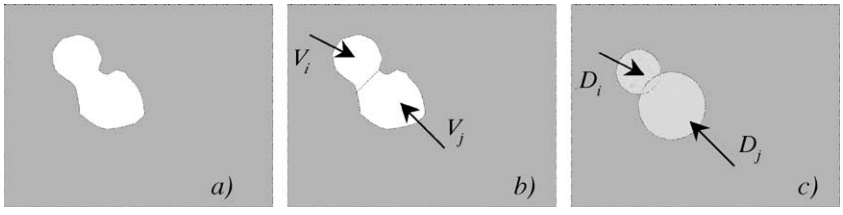

Fig. 3. Approximation of air voids V_k by disks D_k.

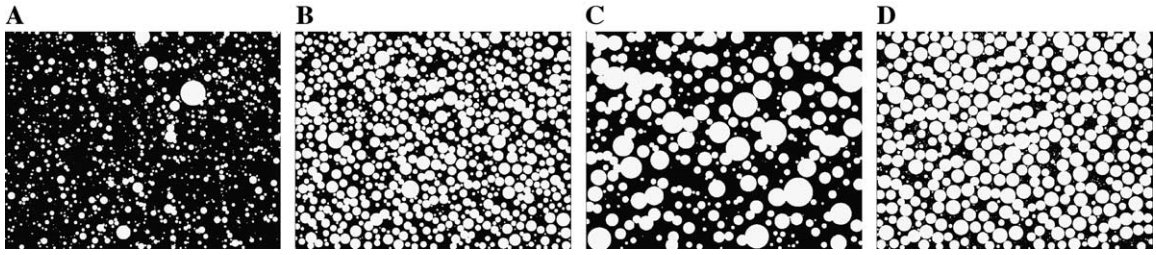

Fig. 4. Results of disk approximation for the voids in Fig. 2.

Since $\delta_A(r)$ is usually given only numerically based on statistical data, (Eq. (2)) cannot be directly used. Therefore, numerical methods have to be used in order to determine $\delta_V(r)$ and N_A using planar information. A classical approach is the Saltykov method, which is based on a discrete approximation of (Eq. (3)), which leads to a system of linear algebraic equations, which can be solved recursively. Details of this method are given in Refs. [18,20]. It is used in this paper for exploring the general form of $\delta_V(r)$, i.e., to come to a family of probability distributions $\delta_V(r;\theta)$, which depend on some parameters, denoted here by a parameter vector θ. However it is, as experience shows, for the given (void) data not precise enough to yield numerical details of $\delta_V(r;\theta)$. So in a second step, the parameter vector θ is estimated by means of the maximum likelihood method [21].

The likelihood function $L(r_1,\ldots r_{n_j};\theta)$ depends on the observed radii r_i of the constructed section disks and the parameter vector θ. It has the form:

$$L\left(r_1,\ldots,r_{n_j};\theta\right)=\prod_{i=1}^{n}\delta_A(r_i;\theta), \tag{4}$$

where $\delta_A(r;\theta)$ is given by the stereological Eq. (3), which contains on its right-hand side the parameterized function $\delta_V(r;\theta)$. For every kind of AAC, four planar sections (sample cube surfaces) offered the data; n is the total number of radii (between 2000 and 5500). The maximum likelihood estimates were then obtained by maximization of $L(r_1,\ldots r_{n_j};\theta)$ for given r_i; in the numerical calculation, the negative logarithm of $L(r_1,\ldots r_{n_j};\theta)$ was minimized by means of the method of steepest descent.

4.2. Void diameter distribution

The stereological exploration based on the Saltykov algorithm led to the following parametric form for $\delta_V(r)$:

$$\delta_V(r)=p_1\delta_{V,1}(r)+p_2\delta_{V,2}(r)+p_3\delta_{V,3}(r) \tag{5}$$

with

$$\delta_{V,i}(r)=\lambda_i e^{-\lambda_1(r-r_0)} \text{ and}$$

$$\delta_{V,3}(r)=\frac{1}{\sigma\sqrt{2\pi}}\exp\left(-\frac{(r-\mu)^2}{2\sigma^2}\right) \text{ for } r\geq r_0,$$

$i=1,2$ and $p_1+p_2+p_3=1$.

That means $\delta_V(r)$ is a mixture of three components with positive weights p_k. The first two components are shifted exponential distributions, which represent two subgroups of very small voids. The third component is Gaussian and corresponds to the larger voids (but not to the huge voids which belong to P_{Cracks}). Perhaps the third component is meant when researchers use Gauss distributions for void radii in AAC [22]. The parameter r_0 is the minimum radius of artificial air pores in the probe.

Fig. 5 shows an approximation of $\delta_V(r)$ for sample D obtained by the Saltykov algorithm. The three-component structure is obvious. In the semi-logarithmical scale, there are two linear components and one parabolic, which are related to the exponential and Gaussian components of $\delta_V(r;\theta)$. Each AAC type is characterized by a parameter vector $\theta=(p_1, p_2, \sigma, \mu, \lambda_1, \lambda_2, r_0)$ of seven independent variables; the values λ_1 and λ_2 (tangents) are presented in Fig. 5.

4.3. Modeling the structure of artificial air voids

It seems to be natural to model the system of voids in AAC as a random system of spheres. As the planar sections of the samples show, there is frequent overlapping of spheres. Thus, a hard-sphere model, as in Ref. [10], is not realistic. On the other hand, it is also not realistic to assume that the spheres are fully penetrable as in the so-called Boolean model [18]. Obviously, the spheres are not fully penetrable: the PCFs of the section disk center systems in

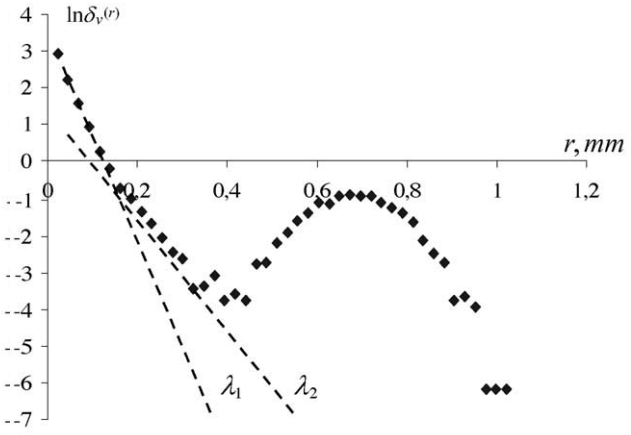

Fig. 5. A rough approximation of $\delta_V(r)$ for sample D obtained by the Saltykov algorithm. The three-component structure is clearly recognizable.

Table 2
Estimated parameters for the four samples and χ^2 values, degrees of freedom and f values

	λ_1	p_1, %	λ_2	p_2, %	μ	σ	p_3, %	r_0, μm	N_A	N_V	f	χ^2	df
A	0.28	46.94	0.25	45.89	9.92	4.13	7.18	23	5496	71845	0,999	5.39	6
B	0.28	44.70	7.18	11.01	19.24	5.34	44.29	70	3062	13936	0,905	11.09	7
C	0.19	21.04	0.07	78.82	18.73	2.02	0.14	70	2087	19401	0,952	16.01	4
D	0.81	63.23	0.33	26.30	29.95	4.45	10.47	23	1972	7292	0,911	7.96	6

Fig. 9 show some form of repulsion between the centers: $g_A(r)$ is smaller than 1 for small r. For a structure with full overlaps, a PCF which is equal to unity for all r is expected. Therefore, the so-called "cherry-pit" model or concentric-shell model seems to be the right model. This model starts with a random system of hard (inpenetratable) spheres (the "pits") and then each of them is surrounded by a soft shell. This model is frequently used in materials science [5,6] and was also successfully applied in concrete research [12]; however, in the concrete application, the pits were really hard objects. In the concrete void context (but not autoclaved aerated concrete), the model appears in Ref. [23].

While the verbal description of the "cherry-pit" model is simple, its mathematical treatment is extremely difficult. In the case of identical "pits", there are some results [5], but for the case of random "pits", simulation is the only way to obtain precise model characteristics. This is also the case for the volume fraction of the system of "cherries", while for the cases of Boolean model and impenetrable spheres, simple formulas exist.

The "cherry-pit" model can be easily simulated if an algorithm for the simulation of the system of pits is available. If such a structure is given, then simply the radii have to be enlarged to the size of the "cherries" without respect to possible overlappings. The method for simulating systems of "pits" used in this paper is the force-based algorithm for the generation of random packings of hard spheres of random radii as described in Refs. [24,25]. This algorithm belongs to the class of collective rearrangement algorithms. From the very beginning, all spheres are present, but initially they may overlap. During the algorithm, the size of the spheres is reduced and the spheres are moved in order to reduce the overlaps until complete non-overlapping is reached. It enables the simulation of very dense packings; for example, for the case of identical spheres, volume fractions until 71% were obtained.

In their simulation of the "cherry-pit" model, the authors used the radius probability density function $\delta_V(r)$ as the probability density function of the "cherry" radii. The radii of the "pits" R_i^{Pit} are of course smaller than those of the "cherry" radii R_i and taken as

$$R_i^{\mathrm{Pit}} = fR_i, \tag{6}$$

where f is a reduction factor. This f is the same for all spheres of a sample, but varies from sample to sample; it is a further model parameter. It is chosen so that the resulting "cherry-pit"

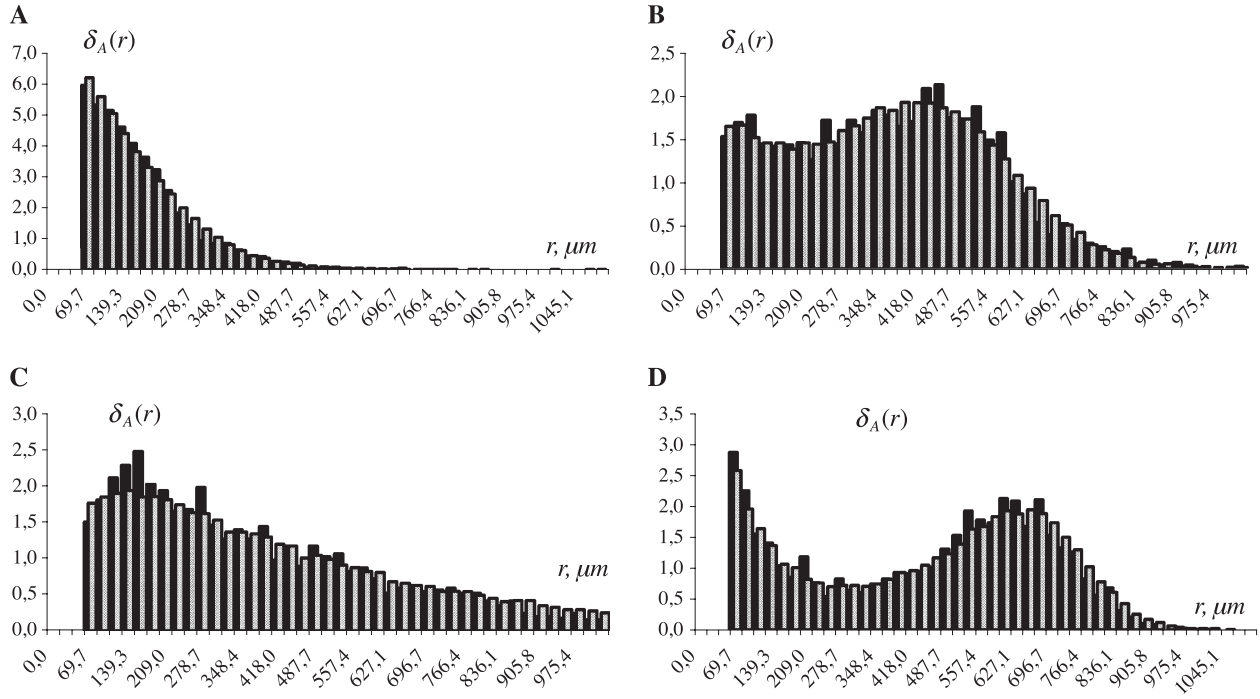

Fig. 6. Experimental and theoretical radius distributions for four samples: filled–experimental 2D distribution; hatched–theoretical distribution in 2D (based on 3D data).

model has the right porosity P_{Air}. Practically, f was obtained by iteration. With some start value of f, a random dense packing wit radii R_i^{Pit} and sphere density N_V was simulated. Then the spheres were extended to the true values R_i and the corresponding porosity was determined. If it is larger than P_{Air}, f was reduced, if smaller, f was increased.

For this paper, planar sections through "cherry-pit" models are important, in particular, the PCF $g_A(r)$ of the centers of section disks. There is nowadays no way to obtain $g_A(r)$ with analytical mathematical methods. An approach leading to $g_A(r)$ could start with the PCF $g_V(r)$ of the centers of the spherical pits. But it is analytically unknown, in the literature, one finds only empirical curves for the case of identical spheres [5]. Then this $g_V(r)$ has to be transformed into $g_A(r)$. Some theory for this step can be found in Ref. [18, Section 11.6], but it is applicable only for the case of identical spheres or spheres with stochastically independent radii; so simulation is the only way for obtaining $g_A(r)$.

5. Results

5.1. Sphere radius distribution parameters

The statistical procedure described in Sections 4.1 and 4.2 yielded for the four samples the parameters given in Table 2.

It shows also χ^2 values belonging to a χ^2 test of goodness-of-fit for the $\delta_A(r;\theta)$ functions. Also, the values of N_V, N_A and f are given. The values of f are close to 1, which shows that the differences to systems of fully impenetrable spheres are not very large.

5.2. Goodness-of-fit of "cherry-pit" model

Of course, it is necessary to test the goodness-of-fit of the "cherry-pit" model. The natural way is to compare planar characteristics of this model, namely the corresponding probability density function of section disk radii $\delta_A(r)$, and the PCF $g_A(r)$ for the disk centers, with their counterparts in the concrete samples. Since the theoretical functions cannot be obtained analytically or numerically, the only way is to simulate the "cherry-pit" model and then to determine the functions statistically. The "cherry-pit" model was simulated in a cubic container of side length 57 mm for the four structures corresponding to Table 2.

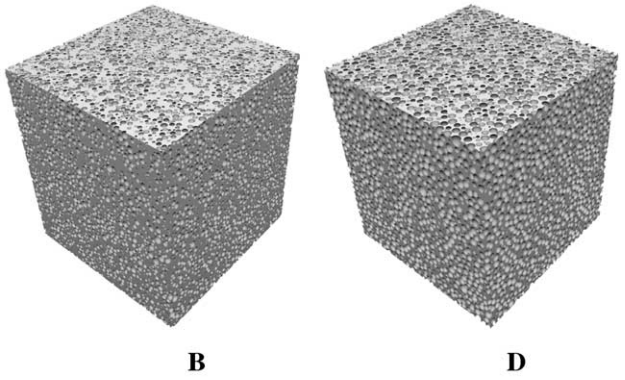

Fig. 8. Simulated samples with parameters as for samples B and D (41 mm side width).

Fig. 6 shows the radius distributions for the disks in planar sections through the simulated 3D structures (Fig. 7) in comparison to the empirical distributions obtained at the surfaces of AAC samples (Fig. 4). In all cases, there is a good agreement between model and experimental values, with small statistical fluctuations. Fig. 8 shows examples of simulated model cubes, which look similarly as their experimental counterparts in Fig. 4.

Finally, Fig. 9 shows the various PCFs $g_A(r)$ corresponding to planar sections: the experimental PCFs for the centers of constructed disks on the surfaces of sampling cubes and analogous functions for the section circle centers of simulated "cherry-pit" models. Also here, the agreement is good. The quantitative differences between the four AAC structures are reflected by different parameters of the "cherry-pit" model as well as by different shapes of PCFs.

6. Evaluation

This paper presents a simple stochastic model for the geometrical structure of the system of artificial air pores in AAC. This model has two ingredients, the pore radius distribution and the "cherry-pit" model. The form of the radius distribution is rather general; three components, two exponential, one Gaussian, offer a great variety of possible distributions. Different weights p_k can lead to qualitatively different distributions; a simple Gaussian distribution seems to be not appropriate. So the authors hope that the suggested radius distribution can be used for many types of AAC.

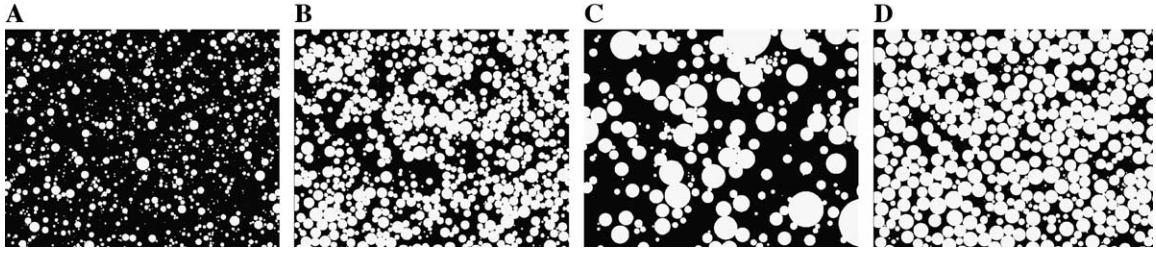

Fig. 7. Cross sections through simulated "cherry-pit" models. Compare with Fig. 4.

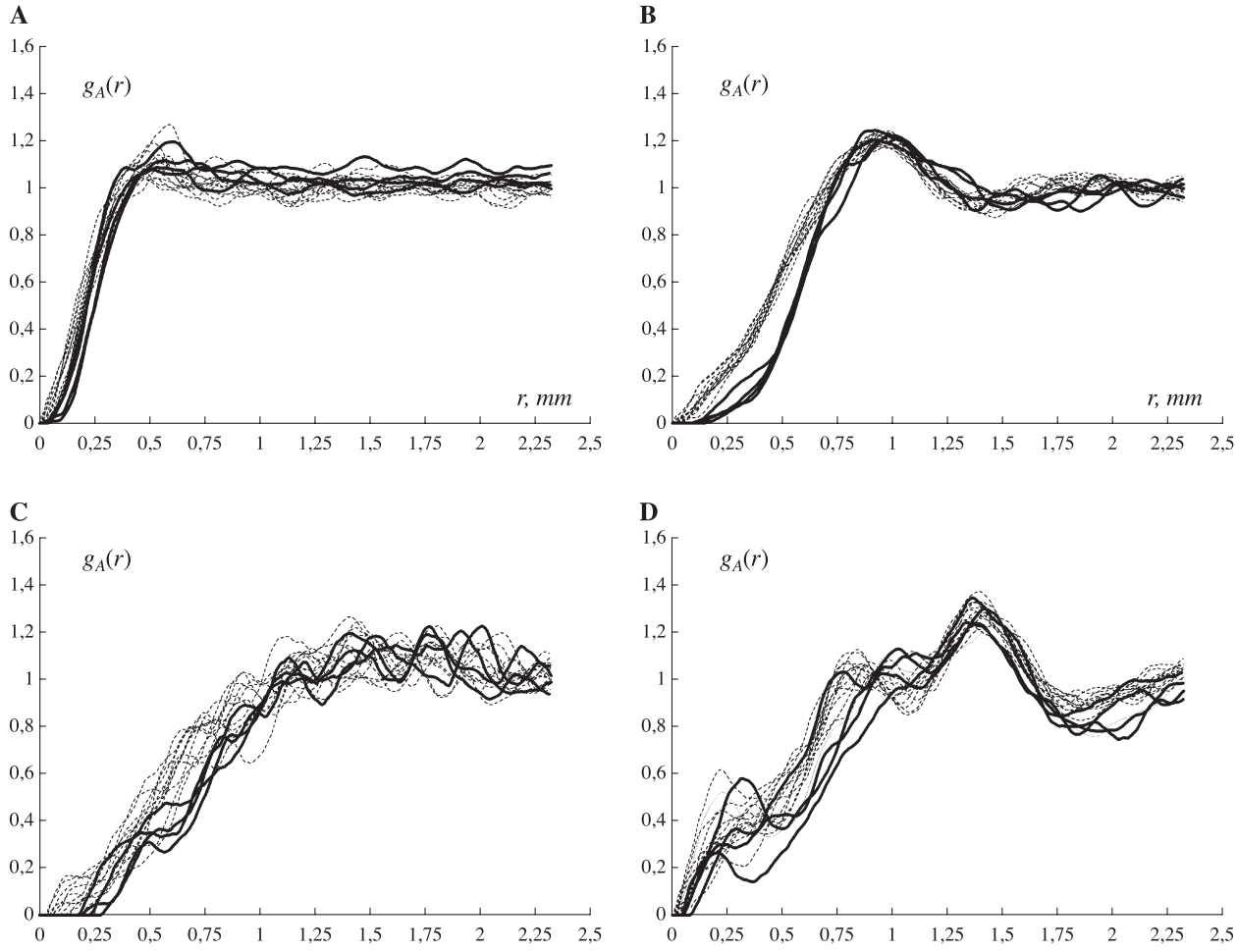

Fig. 9. Pair correlation function $g_A(r)$ for the four AAC types: bold–empirical, from cube surface; normal–theoretical, from planar sections through simulated "cherry-pit" models.

In order to enable comparison to other pore size distributions [3], the density function $\delta_V(r)$ was used for calculating the probability density function of the pore volume distribution $f_V(r)$, which is proportional to $r^3\delta_A(r)$. Fig. 10 shows the relation between the 3D void radius density function and the corresponding pore volume density function. The Gauss component dominates, and there is some similarity to Fig. 5 in Ref. [3].

The "cherry-pit" model is a plausible stochastic structure model, which can be easily simulated. It is more realistic than the hard-sphere packing model of [10] and any form of a Boolean model with fully penetrable spheres. The "cherry-

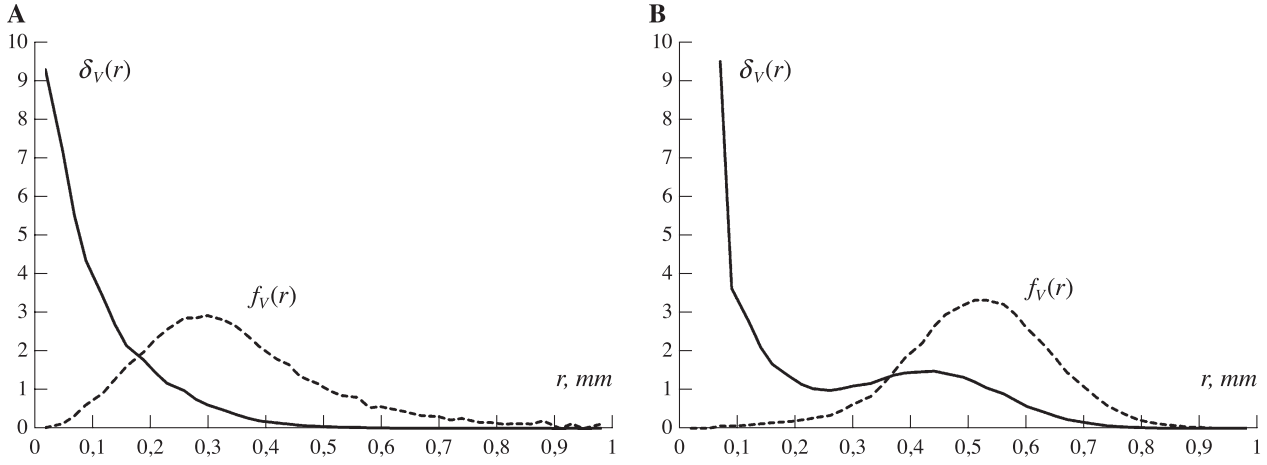

Fig. 10. Radius and pore volume distribution: filled–pore radius distribution; hatched–pore volume distribution.

pit" model is not unknown in concrete research. Bentz et al. [12] used it for ordinary concrete, where the pits stand for the hard particles. So it is a bit of a italics that here a model with 'hard' air bubbles was introduced. By the way, Fagerlund [23] used the model in air void statistics of usual concrete.

The radius distribution is determined by means of a stereological method. A possible alternative could be the use of computerized topography, but personal practical experience of the authors with that method for refractory castables with isolated refractory aggregates of volume fraction around 50% was not encouraging. On the other hand, the nearly spherical form of the pores in the samples observed makes the stereological approach natural and easy to handle.

7. Conclusions

This paper shows that the structure of artificial air pores in AAC can be described by a simple and plausible stochastic model, which was already used for other concrete structures. It has sufficient parameters so that it can be adapted to a broad spectrum of AAC types; perhaps the model is suitable also for other porous building materials. Based on this model, it will be possible to study in high precision bulk properties of AAC such as strength, toughness, heat transfer, moisture transport and others. It is an interesting open question whether the connectivity properties of the model are in agreement with those reported for AAC in Ref. [3].

Acknowledgements

The authors thank the Institute of Ceramics, Glass and Construction Materials, Freiberg University of Mining and Technology, for preparing the raw materials to producing the AAC in the laboratory and Xella Baustoffe for the industrial samples. They are grateful to Mrs. Gudrun Heinzel for technical help in image analysis and gratefully acknowledge the use of the open source image processing library IPL98 (http://www.mip.sdu.dk/ipl98). The constructive remarks of two anonymous referees on an earlier version of this paper were very helpful for improving the exposition. Financial support from the German Science Foundation (DFG) is gratefully acknowledged.

References

[1] P. Prim, F.H. Wittmann, Structure and water absorption of aerated concrete, in: F.H. Wittmann (Ed.), Autoclaved Aerated Concrete, Moisture and Properties, Elsevier, Amsterdam, 1983, pp. 55–69.
[2] S.J. Gregg, K.S.W. Sing, Adsorption, Surface Area and Porosity, Academic Press, London, 1982.
[3] S. Roels, J. Sermijn, J. Carmeliet, Modelling unsaturated moisture transport in autoclaved aerated concrete: a microstructural approach, in: A. Gustavsen, J.V. Thue (Eds.), Proc. 6th Nordic Symposium on Building Physics in the Nordic Countries, vol. 1, Norwegian University of Science and Technology, Trondheim, Norway, 2002, pp. 167–174.
[4] N. Narayanan, K. Ramamurthy, Structure and properties of aerated concrete: a review, Cement and Concrete Composites 22 (2000) 321–329.
[5] S. Torquato, Random Heterogeneous Materials, Microstructure and Macroscopic Properties, Springer, New York, 2002.
[6] M. Sahimi, Heterogeneous Materials, Springer, Heidelberg, 2003.
[7] E. Schlegel, D. Hums, Porenbeton - die Entwicklung von Gefüge und Eigenschaften eines Werkstoffes, Mauerwerk 6 (2002) 82–88.
[8] H. Weber, H. Hullmann, Porenbeton Handbuch, vol. 5, Aufl. Bauverlag, Wiesbaden, 2002.
[9] J.v.d Kooi, Moisture transport in cellular concrete roof, PhD thesis, TU Eindhoven, The Netherlands, 1972.
[10] Tianchun He, Festigkeits- und Verformungsverhalten von Porenbeton, PhD thesis, TU Bergakademie Freiberg, Germany, 1988.
[11] I. Petrov, E. Schlegel, Application of automatic image analysis for the investigation of autoclaved aerated concrete structure, Cement and Concrete Research 24 (1994) 830–840.
[12] D.P. Bentz, E.J. Garboczi, K.A. Snyder, A hard core/soft shell microstructural model for studying percolation and transport, Thee-Dimensional Composite Media, NIST Internal Report 6265, Gaithersburg, Maryland, 1999.
[13] VDI-Wärmeatlas, Berechnungsblätter für den Wärmeübergang, 8.Aufl., Springer, 1997.
[14] E. Schwiete, U. Ludwig, The porosity and the gas permeability of aerated concrete, Proc. Symposium Autoclaved Calcium Silicate Buildings Products, London, 1965.
[15] F.J. Grimer, R.S. Brewer, The within-cake variation of autoclaved aerated concrete, Proc. Symposium Autoclaved Calcium Silicate Buildings Products, London, 1965.
[16] I. Balslev, K. Døring, R.D. Eriksen, Weighted central moments in pattern recognition, Pattern Recognition Letters 21 (2000) 381–384.
[17] J. Hubalkova, D. Stoyan, On a qualitative relationship between degree of inhomogeneity and cold crushing strength of refractory castables, Cement and Concrete Research 33 (2003) 747–753.
[18] D. Stoyan, W.S. Kendall, J. Mecke, Stochastic Geometry and Its Applications, Wiley, Chichester, 1995.
[19] K.A. Snyder, K. Natesaiyer, K. Hover, Stereological and statistical properties of entrained voids in concrete: a mathematical basis for air void system characterization, in: S. Mindess, J. Skalny (Eds.), Proc. Materials Science of Concrete VI, American Ceramic Society, 2001, pp. 129–214.
[20] J. Ohser, F. Mücklich, Statistical Analysis of Microstructures in Materials Science, Wiley, Weinheim, 2000.
[21] J.F. Monahan, Numerical Methods of Statistics, Cambridge University Press, 2001.
[22] T. Schneider, Modellierung der Festigkeit poröser Keramiken, Logos, Berlin, 2002.
[23] G. Fagerlund, Equations for calculating the mean free distance between aggregate particles or air-pores in concrete, CBI Forsknig/Research, vol. 8 (77), Institute of Technology, Stockholm, Sweden, 1977.
[24] A. Bezrukov, M. Bargiel, D. Stoyan, Spatial statistics for simulated packings of spheres, Image Analysis & Stereology 20 (2001) 203–206.
[25] A. Bezrukov, M. Bargiel, D. Stoyan, Statistical analysis of simulated random packings of spheres, Particle and Particle Systems Characterization 19 (2002) 111–118.